WELDING RESEARCH

SUPPLEMENT TO THE *WELDING JOURNAL,* FEBRUARY 2003
Sponsored by the American Welding Society and the Welding Research Council

The Mechanism of Stress-Relief Cracking in a Ferritic Alloy Steel

A novel stress-relaxation technique and extensive microstructural characterization of the carbide precipitation, elemental segregation, and fracture modes were used to investigate stress-relief cracking in a ferritic alloy steel

BY J. G. NAWROCKI, J. N. DuPONT, C. V. ROBINO, J. D. PUSKAR, AND A. R. MARDER

ABSTRACT. Stress-relief cracking is a major cause of weld failures in creep-resistant, precipitation-strengthened materials such as ferritic alloy steels, stainless steels, and Ni-based superalloys. Stress-relief cracking occurs primarily in the coarse-grained heat-affected zone of weldments. Although the general causes of stress-relief cracking are known, the underlying mechanisms are very much a topic of debate. The mechanism of stress-relief cracking in the coarse-grained heat-affected zone (CGHAZ) of a new ferritic alloy steel (HCM2S) was investigated through stress-relaxation testing and detailed microstructural characterization. The CGHAZ simulation and stress-relaxation testing was performed using Gleeble techniques. The time to failure exhibited C-curve behavior as a function of temperature. A balance of intergranular and intragranular carbide precipitation controlled the stress-relief cracking susceptibility. Cracking initiated at prior austenite grain boundaries by cavity nucleation on incoherent, Fe-rich M_3C carbides. The grain interiors were resistant to plastic deformation due to precipitation strengthening by small (5–40 nm) alloy carbides. Elemental segregation played no detectable role in the stress-relief cracking failures. Much of the microstructural characterization was performed using a VG603 FEG STEM having a probe size of about 1.5 nm. The small probe size allowed nano-sized precipitates to be individually analyzed by using EDS and elemental EDS traces taken across prior austenite grain boundaries. In addition, SE STEM imaging with the VG603 FEG STEM was able to resolve small precipitates that were previously unobservable using conventional TEM and STEM techniques. The results of this study form a basis for heat treatment and welding process variables for HCM2S to avoid stress-relief cracking. In addition, these procedures and analytical results can be applied to other materials to avoid microstructures that are susceptible to stress-relief cracking.

J. G. NAWROCKI, A. R. MARDER, and J. N. DuPONT are with Department of Materials Science and Engineering, Lehigh University, Bethlehem, Pa. C. V. ROBINO and J. D. PUSKAR are with Joining and Coating Department, Sandia National Laboratories, Albuquerque, N.Mex.

Introduction

Ferritic alloy steels such as 2.25Cr-1Mo steel are commonly used for high-temperature applications in steam generators and pressure vessels for chemical and fossil power plants. Many components in these power plants operate at temperatures of approximately 300–700°C. New components fabricated from 2.25Cr-1Mo steel may require welding at both the installation and fabrication stages, and in-service material may be welded during repairs. In such applications, preheat and/or postweld heat treatments (PWHT) are often required to improve heat-affected zone (HAZ) mechanical properties and reduce susceptibility to hydrogen cracking. These preheat and PWHT steps represent a significant fraction of the overall fabrication/repair costs.

Recently, a new ferritic steel, denoted as HCM2S, was developed. HCM2S has been reported to exhibit improved mechanical properties and resistance to hydrogen cracking compared to 2.25Cr-1Mo steel (Refs. 1, 2). Table 1 compares the allowable composition ranges of both 2.25Cr-1Mo steel and HCM2S. Although the carbon content of HCM2S and 2.25Cr-1Mo can be identical, HCM2S is typically produced with a carbon content of ~0.06 wt-%, which is much lower than the typical carbon content of 2.25Cr-1Mo steel (Refs. 1–5). In addition, the maximum allowable C content is 0.1 and 0.15 wt-% for HCM2S and 2.25Cr-1Mo steel, respectively. The lowered carbon content of HCM2S relative to 2.25Cr-1Mo steel improves weldability by reducing hardenability and, therefore, the as-welded hardness of the HAZ. The creep rupture strength is improved by the substitution of Mo with W as a solid solution strengthener. Vanadium and niobium are added to improve creep strength by way of carbide precipitation strengthening. Boron is also added to improve creep strength. It has recently been suggested that the improved weldability from these composition modifications may permit elimination of costly preheat and/or PWHT requirements (Ref. 1). However, even if no PWHT is necessary, HCM2S will be exposed to comparable temperatures in service

KEY WORDS

Stress-Relief Cracking
Carbide Precipitation
Coarse-Grained HAZ
Heat-Affected Zone
Ferritic Alloy Steel
High Temperature

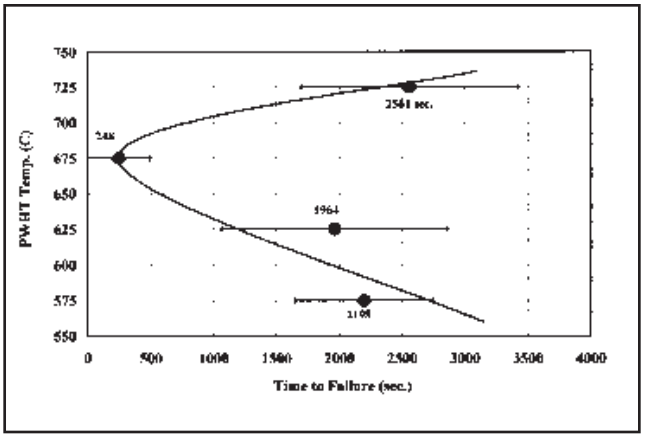

Fig. 1 — Time to failure during stress-relaxation testing for various test temperatures. The numbers within the graph represent the average of four to six tests at temperature.

Table 1 — Allowable Composition Ranges of HCM2S (wt-%)

Element	HCM2S (Ref. 1)	2.25Cr-1Mo (Ref. 3)
C	0.04–0.10	≤0.15
Cr	1.90–2.60	2.00–2.50
Mo	≤0.30	0.90–1.10
W	1.45–1.75	—
V	0.20–0.30	—
Nb	0.02–0.08	—
B	≤0.006	—
Al	≤0.03	—
Si	≤0.50	0.20–0.50
Mn	0.30–0.60	0.30–0.60
P	≤0.030	≤0.035
S	≤0.010	≤0.035

Table 2 — Chemical Composition of HCM2S Used in this Research

Element	Wt-%
C	0.061
Cr	2.52
Mo	0.11
W	1.50
V	0.24
Nb	0.05
B	0.0036
Al	0.013
Si	0.30
Mn	0.33
Ni	0.07
N	0.007
P	0.0013
S	0.006
Ar	0.0029
Sb	0.0001
Sn	0.007
Cu	0.022

where stress-relief cracking can occur during operation (Refs. 1, 2). In addition, HCM2S may be welded to existing 2.25Cr-1Mo steel that requires a PWHT. Previous work has shown HCM2S to be susceptible to stress-relief cracking, but the underlying mechanisms are largely undetermined (Ref. 6).

Stress-relief cracking is a common cause of weld failures in many creep-resistant, precipitation-strengthened alloys such as ferritic alloy steels (Refs. 7–9), stainless steels (Refs. 10, 11), and Ni-based superalloys (Refs. 12, 13). The general definition of stress-relief cracking is intergranular cracking in a welded assembly that occurs during exposure to elevated temperatures produced by post-weld heat treatments (PWHT) or high-temperature service (Ref. 14). Residual stresses are typically relieved during a PWHT through plastic deformation of the material. Therefore, a susceptible microstructure is one with strong grain interiors that resist plastic deformation and weak grain boundaries. Failure can occur in the heat-affected zone or fusion zone, but the coarse-grained heat-affected zone (CGHAZ) is the most susceptible region of a steel weldment.

Although the details of stress-relief cracking mechanisms are not totally understood, general knowledge of the causes of stress-relief cracking for ferritic alloy steels has been well developed (Refs. 8, 14–17). During a typical arc welding process, the unmelted base metal directly adjacent to the fusion zone reaches temperatures close to the melting point of the material, high in the austenite phase field of the Fe-C phase diagram. During the time spent in the austenite phase field, pre existing carbides, nitrides, carbonitrides, and even some inclusions dissolve into the austenite matrix. Since dissolution of the precipitates is diffusion-controlled, the degree of dissolution is dependent on the welding parameters that influence the thermal profile (time and temperature). However, if sufficient dissolution occurs, austenite grains grow essentially unimpeded, resulting in a large austenite grain size. Due to the fast cooling rates associated with arc welding, dissolved alloying elements remain trapped in solution and the austenite transforms to low-ductility martensite or bainite depending on the hardenability and thermal cycle. Another possibility is that the newly formed martensite may auto-temper during cooling, which is favored in systems with high martensite start and finish temperatures.

Carbides begin to precipitate when the CGHAZ is exposed to elevated temperatures during postweld heat treatment for stress-relief and/or during service. Eventually, stable carbides such as those based on V, Mo, Nb, and W nucleate on the many dislocations present in the grain interiors. The result is a fine, uniform dispersion, producing significant precipitation strengthening and even secondary hardening. These alloy carbides are mainly coherent or semicoherent with the ferrite matrix and stable at relatively high temperatures for long times (Refs. 7, 8, 14). The precipitates retard dislocation movement and restrict relaxation of residual stresses during postweld heat treatment. Carbides will also form on the energetically favorable prior austenite grain boundaries. These carbides are typically Fe_3C, $M_{23}C_6$, and M_6C and, at later stages of coarsening, are mainly incoherent with the matrix. They coarsen easily due to the incoherency and the fact they are located along high diffusivity paths. The matrix adjacent to the boundaries can then become devoid of alloying elements, and a precipitate-free or denuded zone is thereby formed along the prior austenite grain boundary (Refs. 9, 11). This region is soft and ductile relative to the remaining precipitation-strengthened grain interior.

Elemental segregation is also known to cause stress-relief cracking (Refs. 14, 15). Tramp elements (S, P, Sn, Sb, As) and intentionally added elements (Al, B, Mn) can segregate to prior austenite grain boundaries causing decohesion and weakening of the boundaries. In addition, sulfides are thought to precipitate at prior austenite grain boundaries, act as cavity nucleation sites, and promote crack propagation through stress-driven diffusion (Ref. 18).

The result of the above microstructural features is a precipitation-strengthened matrix with comparatively weak grain boundary areas caused by one or more of the following: coarse, incoherent precipitates; a soft denuded zone; and/or elemental segregation. Therefore, stress (residual or applied) will not be relieved through the intended macroscopic plastic deformation of the grains, but rather by cracking along prior austenite grain boundaries culminating in catastrophic, stress-relief cracking failure.

As described above, numerous theories exist on the causes of stress-relief cracking and these theories may all be valid under certain circumstances. The general reasons for stress-relief cracking are known, but the underlying mechanisms are still a source of debate. Many studies explore only one mechanism and disregard others. In addition, various

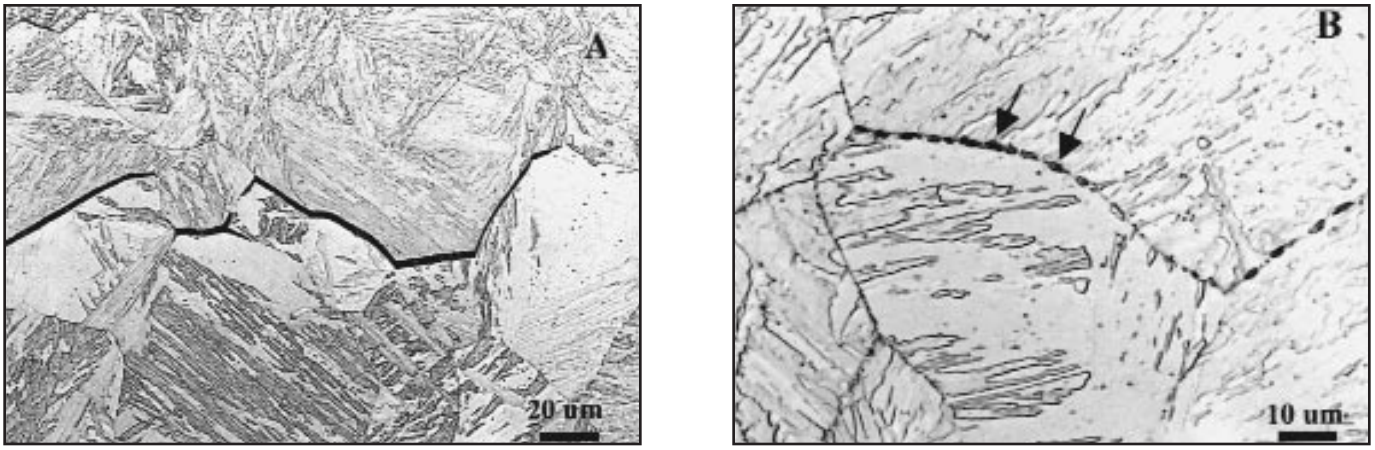

Fig. 2 — Representative LOM photomicrographs of failed samples viewed in cross section. Arrows indicate areas of void formation.

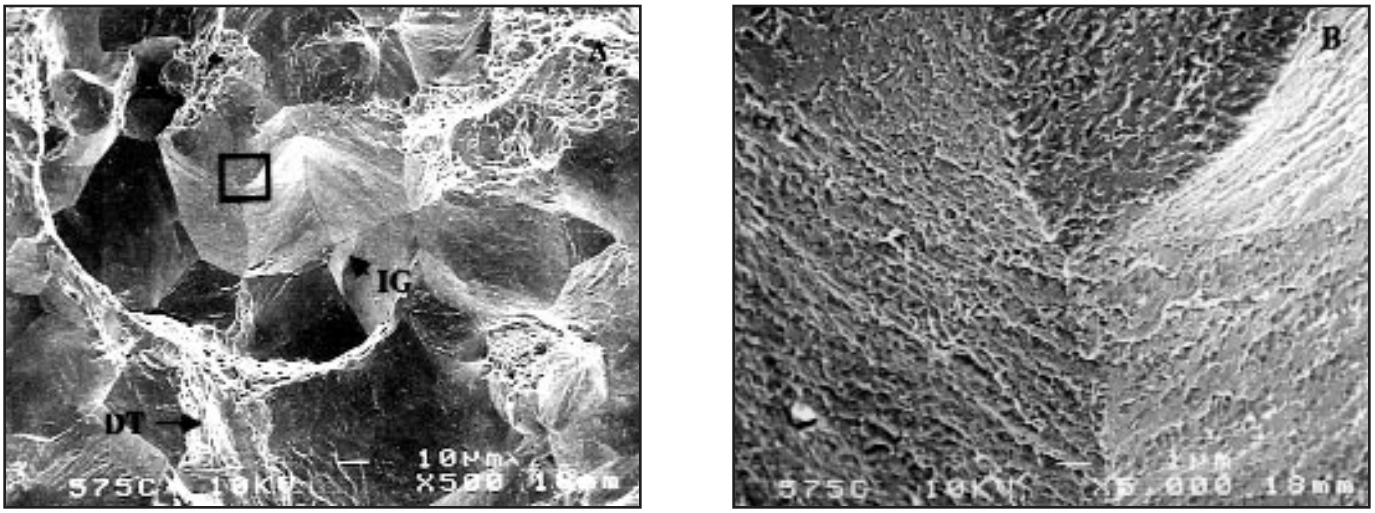

Fig. 3 — Representative SEM photomicrographs of the fracture surface of a sample that failed during testing at 575°C. IG = region of intergranular fracture; DT = region of ductile tearing.

mechanisms can operate simultaneously and the mechanism can change as a function of temperature.

The alloy HCM2S may be susceptible to stress-relief cracking from a compositional standpoint because it contains many strong carbide-forming elements and elements known to embrittle grain boundaries. Previous studies have confirmed HCM2S can be susceptible to stress-relief cracking (Ref. 6). Therefore, the objective of this research was to gain a fundamental understanding of the mechanism(s) of stress-relief cracking using HCM2S as the model system. Although HCM2S is a complicated system, such an alloy is necessary to explore each of the possible mechanisms of stress-relief cracking. Conclusions of this research will form a basis for heat treatment and welding processing variables necessary to avoid a microstructure susceptible to stress-relief cracking in ferritic alloy steels and other susceptible alloys.

Experimental Procedure

The chemical composition of the HCM2S used in this work, as determined using optical emission spectroscopy and wet chemical analysis, is shown in Table 2. Constant displacement, stress-relaxation tests were conducted to assess the stress-relief cracking susceptibility of the CGHAZ of HCM2S using round samples with a length of approximately 105 mm and a diameter of 10 mm with threaded ends. The samples had a reduced gauge-section approximately 10 mm in length and 5 mm in diameter. The CGHAZ was simulated and all testing was done using a Gleeble 1000 thermomechanical simulator. The thermal cycle to produce the CGHAZ was representative of the following weld parameters: 2 kJ/mm energy input, 93°C preheat temperature, and a peak temperature of 1350°C for a 12.7-mm steel plate (Refs. 19, 20). The samples were then cooled to room temperature and heated to the desired PWHT temperature at a rate of 200°C/s. The simulated CGHAZs were tensile tested at temperatures of 575, 625, 675, and 725°C to obtain the necessary data for the stress-relaxation tests. The 0.2% offset yield point was determined from the tensile tests using a dilatometer, which allowed only the CGHAZ to be monitored during tensile testing. The corresponding lengthwise displacement at the 0.2% yield point was determined from the acquired data and then used for the constant displacement stress-relaxation tests because the Gleeble could not be programmed to pull the sample to the required cross-wise displacement. Further details of the stress-relaxation test procedure can be found in (Ref. 21).

The stress-relaxation tests were done as follows: The CGHAZ was simulated as described above, cooled to room temperature and heated to a programmed PWHT temperature of 575, 625, 675, or 725°C. The samples were loaded in tension to the

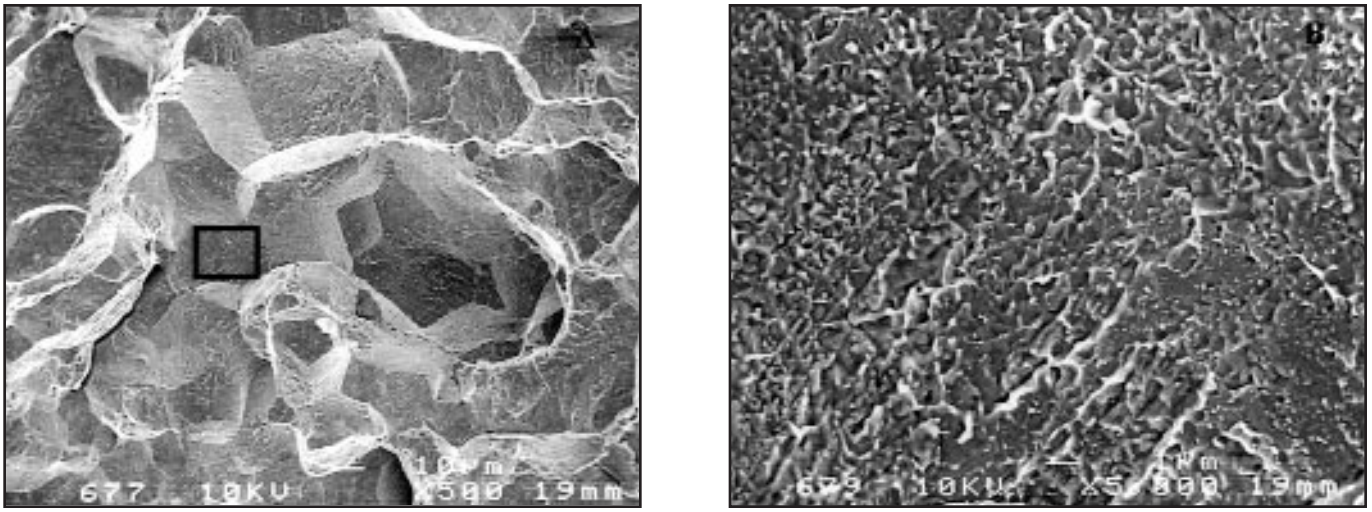

Fig. 4 — Representative SEM photomicrographs of the fracture surface of a sample that failed during testing at 675°C.

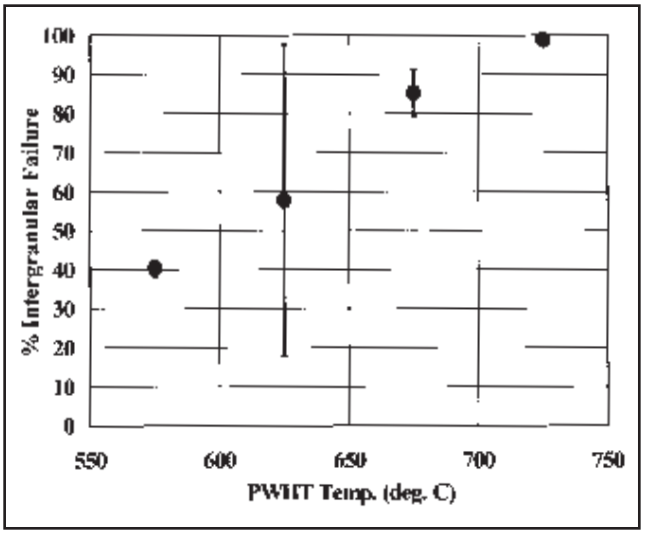

Fig. 5 — Amount of intergranular failure as a function of temperature.

displacement value corresponding to the 0.2% offset yield strength of the CGHAZ determined from tensile testing at temperature. The displacement was then held constant and the load was monitored as a function of time. This test method effectively simulates the residual stresses present in an actual weldment because the maximum residual stress that can be present is the yield strength (Ref. 22). Four to six stress-relaxation tests were performed per temperature and the times to failure obtained from the acquired data.

Failed samples were examined using light optical microscopy (LOM), scanning electron microscopy (SEM), and transmission electron microscopy (TEM). Samples were prepared using standard metallographic techniques and viewed in cross-section using light optical microscopy. The fracture surfaces were examined using a JEOL 6300f SEM operated at 10 kV. Thin foils were prepared by mechanically grinding 3-mm-diameter disks to ~50 μm followed by ion beam thinning to electron transparency. Elemental segregation was examined in thin foils by performing EDS linescans across prior austenite grain boundaries with a VG603 FEG STEM. The VG603 FEG STEM is a very unique instrument due to the very high beam current produced in a small area. The beam size is only ~1.5 nm and the accelerating voltage is 300 kV. These features allow very small areas of a sample to be analyzed without long counting times or sacrificing resolution. In addition, the small beam size allows the boundary to be analyzed with minimum interference from the matrix on either size of the boundary. Carbide precipitation was analyzed using carbon extraction replicas. The carbides were analyzed using EDS and convergent beam electron diffraction using both a JEOL 2000FX TEM operating at 200 kV and the previously mentioned VG603 FEG STEM. Secondary electron (SE) STEM imaging in the VG603 FEG STEM was used to resolve small precipitates on the carbon extraction replicas. These precipitates were unresolvable using conventional TEM and STEM techniques. Similar work, especially with regard to stress-relief cracking, had not been performed prior to this study.

Results and Discussion

Stress-Relaxation Tests

The stress-relief cracking susceptibility was measured by the time to failure during stress-relaxation testing. The time to failure as a function of temperature exhibited C-curve behavior as shown in Fig. 1. The nose of the C-curve, or shortest time to failure, occurred at 675°C. Typical light optical micrographs (cross-sectional view) of failed samples are shown in Fig. 2A and B. Many cracks are present behind the fracture edge. These cracks always occurred along prior austenite grain boundaries approximately normal to the tensile axis. Away from the fracture surface, cracks were never observed transgranularly or along packet boundaries. Cavities were also observed along the prior austenite grain boundaries, as illustrated in Fig. 2B. Thus, the general failure characteristics of the stress-relief cracking simulations are similar to those encountered in actual weldments.

The microscopic failure mode was further investigated using scanning electron microscopy to examine the fracture surfaces. The failure mode was strongly a function of test temperature. Figures 3 and 4 are representative scanning electron micrographs of the fracture surfaces of samples that failed during testing at 575 and 675°C, respectively. The samples tested at 575°C exhibited both intergranular failure (IG) and conventional macroscopic ductile tearing (DT), as shown in Fig. 3A. Examination of the areas of intergranular failure at higher magnification shows significant microductility (localized ductile failure comprised of microvoids) is present on the grain faces and possibly some small particles are also present on the grain faces — Fig. 3B. In contrast, the

samples tested at 675°C failed almost completely intergranularly — Fig. 4A. The exposed grain surfaces were covered with microductility and small particles similar to the samples tested at 575°C — Fig. 4B. The amount of intergranular failure was measured from scanning electron photomicrographs using an image analysis system. In general, the amount of intergranular failure increased with increasing test temperature, as illustrated in Fig. 5. Samples tested at 575 and 625°C had only 40–60% intergranular failure, while those samples tested at 675 and 725°C exhibited 80–100% intergranular failure. These results imply the prior austenite grain boundary characteristics change with temperature and, therefore, further analysis of the grain boundaries was conducted.

Elemental Segregation

EDS linescans were done across prior austenite grain boundaries on thin foils prepared from samples that failed during stress-relaxation testing to determine if elemental segregation, in particular if known embrittling elements (S, P, Sn, As, Sb, and Mn), contributed to stress-relief cracking. Multiple boundaries (at least three) were analyzed in each sample and multiple linescans (at least two) were performed at different locations across a given boundary. Linescans were done by "stepping" the beam across prior austenite grain boundaries. Approximately 64 steps were done per linescan in increments of approximately 1 nm. The boundary could be analyzed with minimal interference from the matrix on either side of the boundary because the beam size was only ~1.5 nm. In addition, the beam current was high enough that a sufficient number of counts could be collected in a small amount of time, which minimized specimen drift. The results from typical EDS linescans are shown in Fig. 6, although not every element analyzed is shown. The STEM photomicrographs show the boundaries analyzed. The arrow on the photomicrograph indicates the direction of the EDS linescan (left to right on the graphs below the photomicrographs), and the "dotted" line to the left of the arrow on the photomicrograph shows, by virtue of the intense beam current, the path along which the beam traveled — Fig. 6A only. The graphs shown below the photomicrograph represent the number of X-ray counts as a function of distance or position for a given element. The prior austenite boundary position is

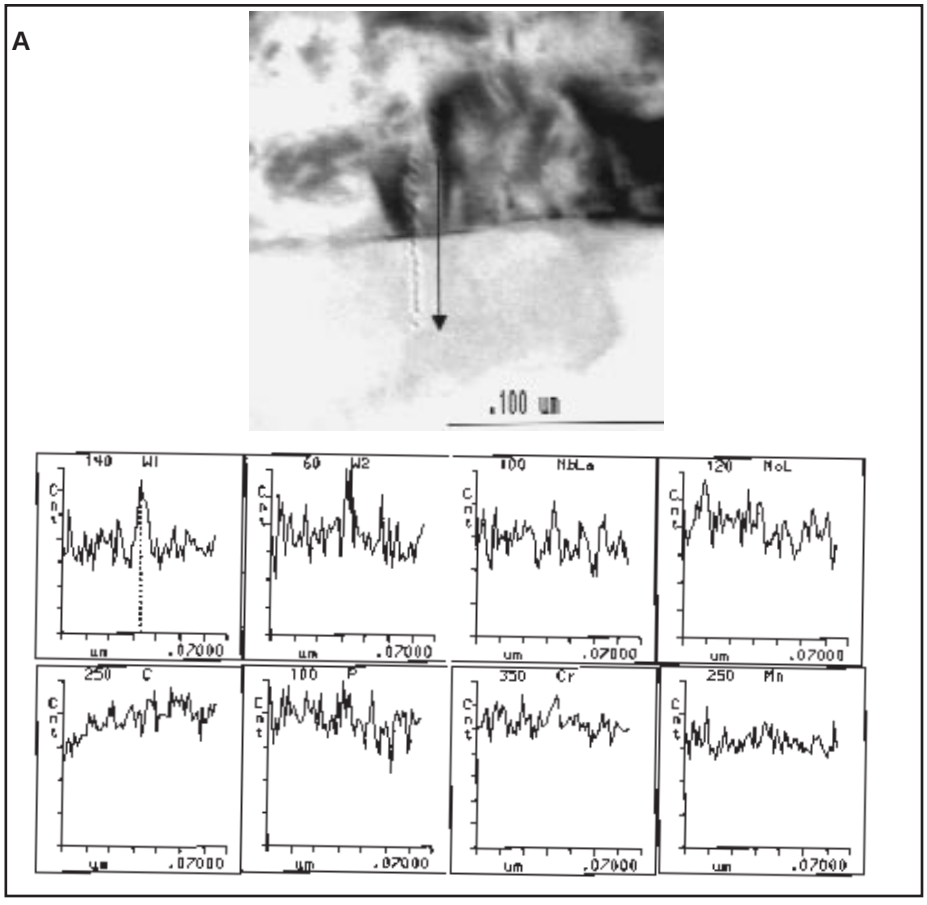

Fig. 6 — Typical EDS line scans done across prior austenite grain boundaries. Dotted line on W1 represents boundary position. A — Sample tested at 675°C; B — sample tested at 725°C.

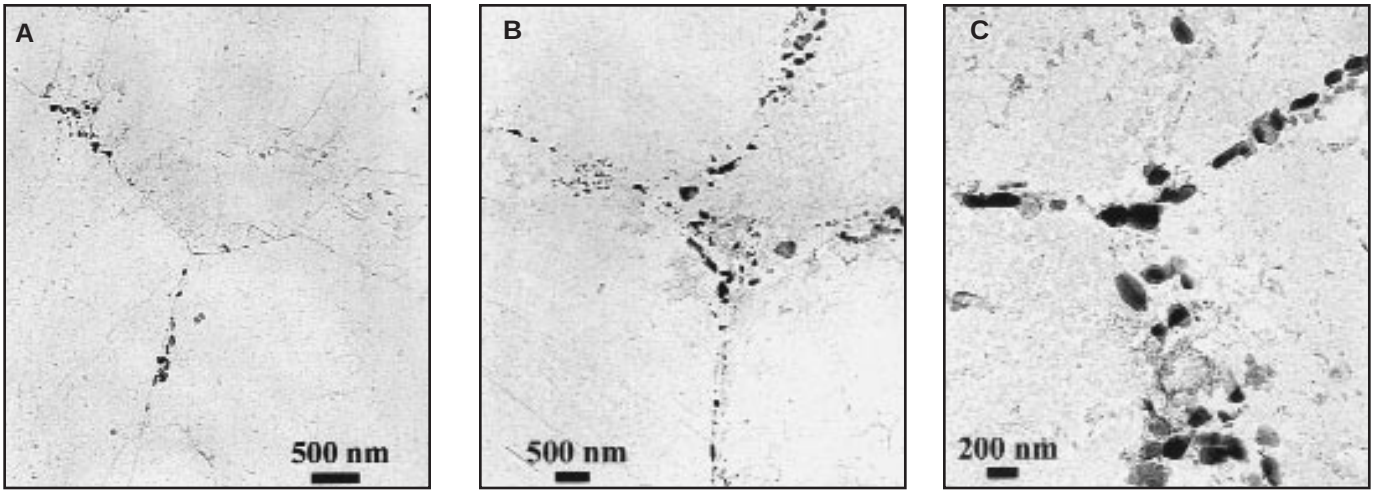

Fig. 7 — TEM photomicrographs of extraction replicas of typical prior austenite grain boundaries in a sample failed after testing. A — 575°; B — 675°C; C — 725°C.

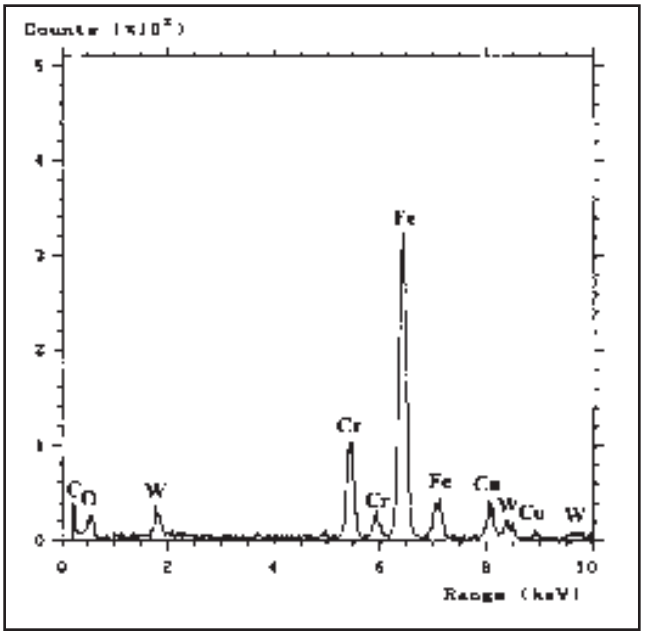

Fig. 8 — Representative EDS spectrum of Fe-rich M_3C found along prior austenite grain boundaries in the CGHAZ of failed stress relief cracking samples. Sample tested at 675°C.

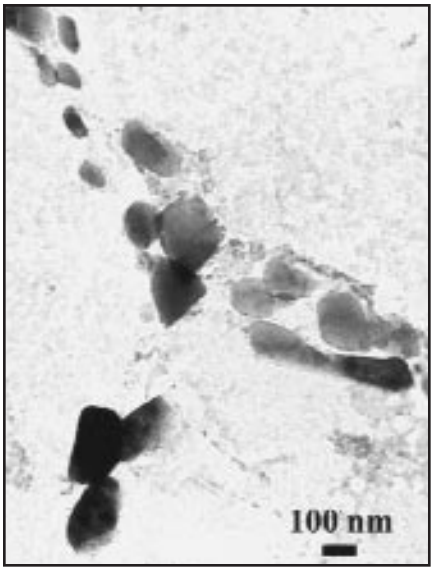

Fig. 9 — TEM photomicrographs of extraction replicas of a typical prior austenite grain boundary triple point containing many coarse, incoherent M_3C carbides. Sample tested at 675°C.

indicated by the dotted line in the first graph of tungsten (W1). The only element enriched at the prior austenite grain boundary is W. Although it may appear an element such as Cr is also enriched at the prior austenite grain boundary (Fig. 6A), a calculation to indicate statistical significance (Ref. 23) shows W is the only statistically significant element enriched at the prior austenite grain boundary. Tungsten enrichment was found at almost every prior austenite grain boundary at each test temperature. Chromium and V segregation were occasionally observed, such as in Fig. 6B, but no tramp element segregation was detected at any prior austenite grain boundary. Again, it appears P is enriched at the prior austenite grain boundary, but the peak is statistically insignificant.

Tungsten has been shown to segregate to prior austenite grain boundaries in ferritic alloy steels (Ref. 24), but was found to de-embrittle the grain boundaries. In addition, much microductility was found on the areas of intergranular failure on the fracture surfaces. This characteristic fracture surface is not typical of failure due to tramp element segregation where the areas of intergranular failure have smooth and featureless fracture surfaces. It can be concluded from these results that elemental segregation did not contribute to stress-relief cracking in HCM2S. However, it should be noted boron segregation, which has been linked to stress-relief cracking in some alloys (Refs. 14, 15), couldn't be reliably detected by the analytical methods used here.

Carbide Precipitation

Transmission electron microscopy was used to further analyze the prior austenite grain boundaries. Carbides were identified using convergent beam electron diffraction patterns and from their characteristic EDS spectra (Refs. 25–27). Typical TEM extraction replica photomicrographs of prior austenite grain boundaries observed in samples tested at 575, 675, and 725°C are shown in Fig. 7. Carbides are visible along the prior austenite grain boundaries. These carbides ranged in size from about 50 to a few hundred nanometers and were identified as Fe-rich M_3C carbides with a representative EDS spectrum shown in Fig. 8. The samples tested at 575°C did not contain carbides at each prior austenite grain boundary — Fig. 7A. In contrast, the prior austenite grain boundaries of the samples tested at 675°C are more fully covered by the M_3C carbides (Fig. 7B), and the boundaries in Fig. 7C (725°C) are almost completely covered. The amount of grain boundary coverage as a function of temperature could

not be quantified, but, in general, the amount of grain-boundary carbides (area fraction or % of grain boundary area covered) increased with increasing temperature. The varying coverage along a given grain boundary is probably due to orientation mismatch between adjacent grains. In general, increasing the degree of misorientation (less coincident sites) makes the site more energetically favorable to carbide precipitation because grain-boundary energy increases with misorientation (Ref. 28). As the temperature (or time) is increased, the degree of misorientation plays less of a role (Ref. 29). The varying degree of misorientation is presumably the reason almost every prior austenite grain boundary in the samples tested at 675°C were covered with carbides.

Further examination of the grain-boundary carbides explains their role in the stress-relief cracking failures. Figure 9 is a higher magnification view of a typical prior austenite grain boundary triple point containing many Fe-rich M_3C carbides. Most of these carbides have curved interfaces and are relatively coarse. In addition, M_3C car-

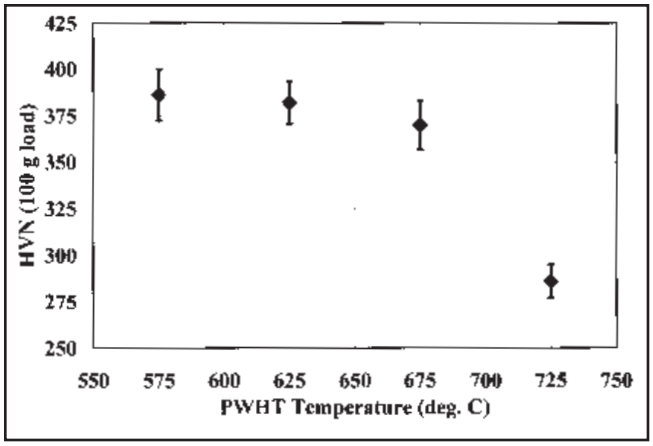

Fig. 10 — Intragranular hardness as a function test temperature.

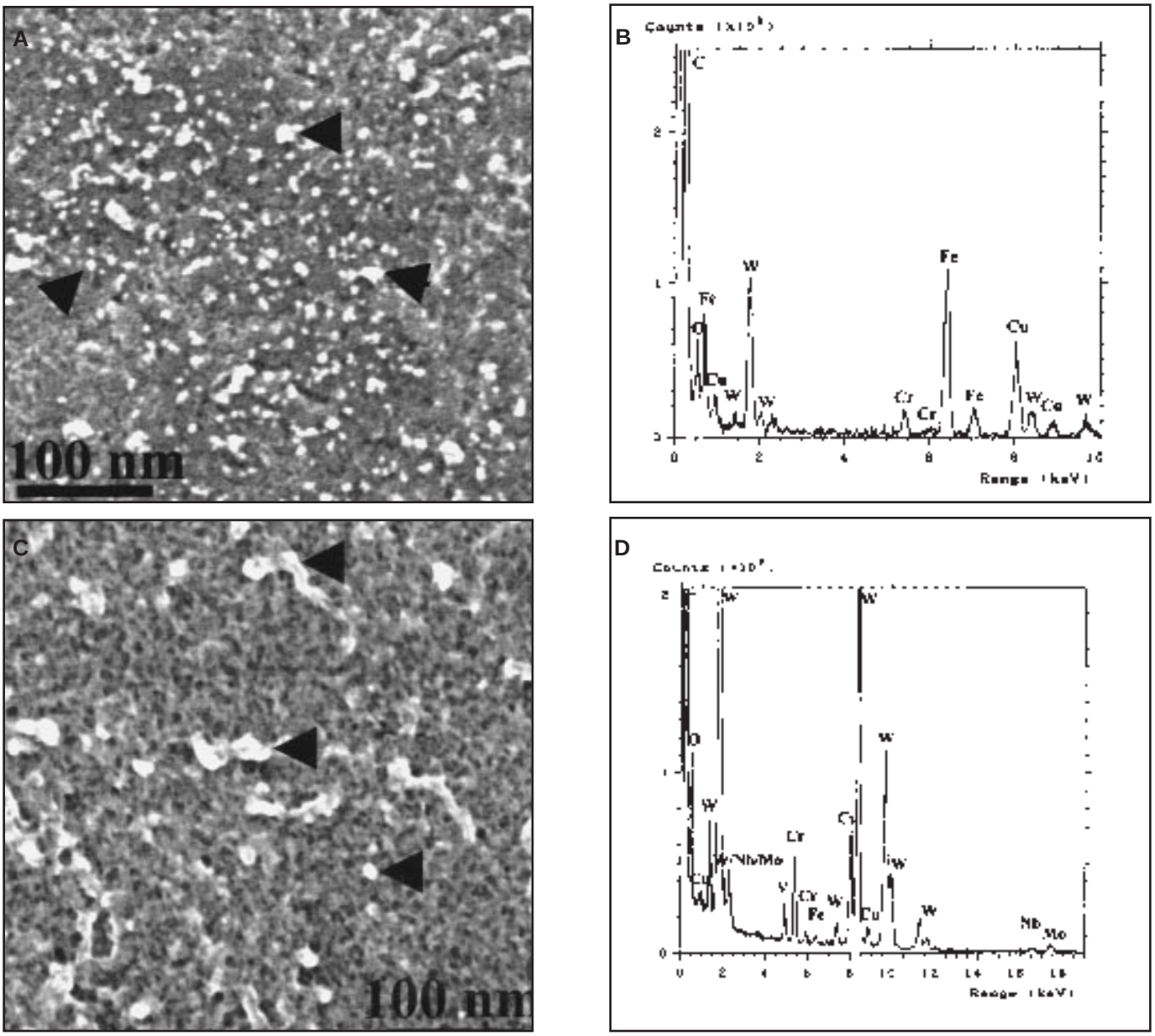

Fig. 11 — STEM photomicrographs of extraction replicas of typical intragranular regions of samples that failed during stress-relief cracking testing and accompanying EDS spectra. A — A dense distribution of W/Fe-rich carbides, sample tested at 575°C; B — representative EDS spectrum; C — dense distribution of W-rich carbides, sample tested at 675°C; D — representative EDS spectrum.

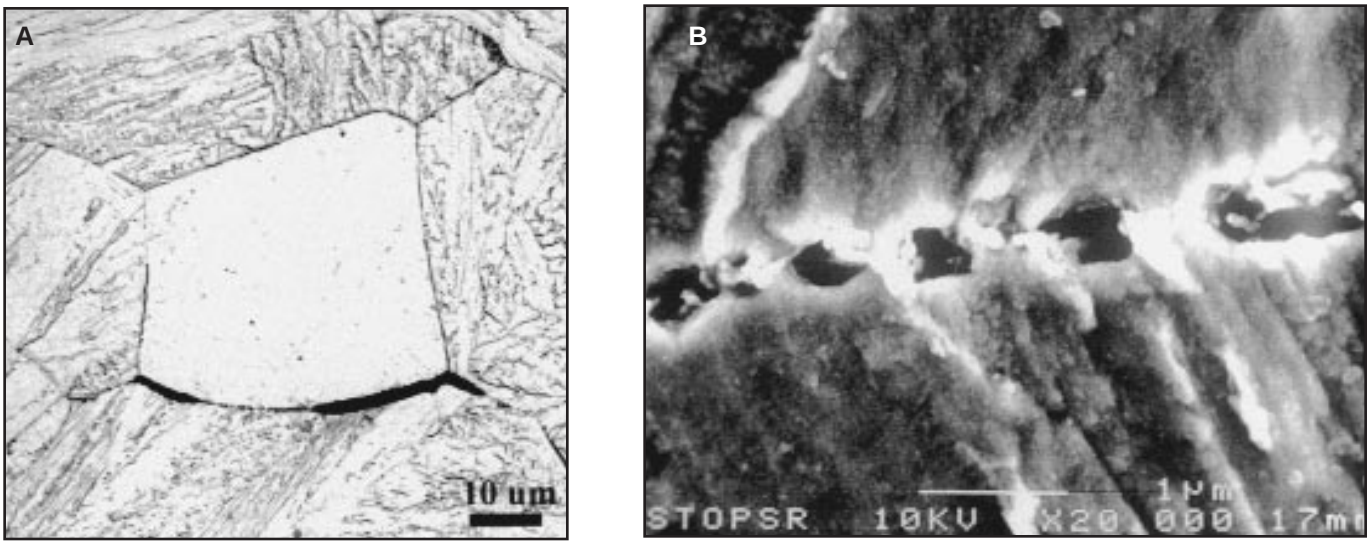

Fig. 12 — Example of crack and cavity formation at a prior austenite grain boundary. The cavities have nucleated on incoherent M_3C carbides. A — LOM photomicrograph; B and C — SEM photomicrographs.

bide has the orthorhombic crystal structure and, therefore, has little coherency with the bcc/bct ferrite matrix. The amount of intergranular failure increased with increasing temperature due to increasing amounts of intergranular M_3C carbides. However, if only grain- boundary carbides controlled stress-relief cracking, the time to failure would be expected to decrease with increasing temperature because the amount of grain-boundary carbides and intergranular failure increased with increasing temperature. However, the time to failure did not increase with temperature but exhibited C-curve behavior, as shown in Fig. 1. Thus, another factor is contributing to the stress-relief cracking failures.

Stress-relief cracking is a function of the material's ability to plastically deform to accommodate residual or service stresses. The strength of the prior austenite grain interiors largely governs the ability to plastically deform globally. Hardness measurements were taken on samples after stress-relaxation failure. The indents were placed only within the prior austenite grain interiors to minimize any contribution from the prior austenite grain boundaries and the results shown in Fig. 10. The hardness (resistance to plastic deformation) is approximately equal for the samples tested at 575, 625, and 675°C, but is significantly less in the sample tested at 725°C. It should be noted the use of a room temperature mechanical test to understand elevated temperature deformation is not entirely appropriate. These hardness tests were done at room temperature. The deformation mechanisms in most alloys differ between room temperature and elevated temperature. For instance, at elevated temperatures, dislocation climb and slip occur, but at room temperature, only slip typically occurs (Ref. 3). In addition, stress-relief cracking is a time-dependent failure, but hardness testing is time independent. Nevertheless, microstructural features such as precipitates, which provide obstacles to deformation, are likely to affect the deformation response in a qualitatively similar manner at high and low temperatures. Thus, the room-temperature hardness test should provide a reasonable representation of the relative strength of the grain interiors.

Carbide precipitation and, to a lesser extent, dislocation density, control the strength of the grain interiors. The morphology and coherency are the main factors that determine the strengthening potency of the precipitates. TEM and STEM techniques were used to examine intragranular precipitation as a function of test temperature. Figure 11A is a secondary electron (SE) STEM image of a carbon extraction replica of a typical intragranular region in a sample tested at 575°C. SE STEM imaging allows for the topography of a sample to be examined, and, therefore, small particles on a film are easily observed. These small particles were unobservable using conventional TEM imaging. A dense distribution of small precipitates is visible in Fig. 11A. These precipitates were found to be W and/or Fe-rich carbides that varied in size from approximately 5–20 nm with a representative EDS spectrum of an individual precipitate shown in Fig. 11B. Individual carbides were able to be analyzed using a VG603 FEG STEM because the beam size is only about 1.5 nm. These W/Fe-rich carbides provided significant precipitation strengthening that resulted in the relatively high hardness shown in Fig. 10. A SE STEM image of a typical intragranular region in a sample tested at 675°C is shown in Fig. 11C. A dense distribution of precipitates about 5–40 nm in size is present. These precipitates were found to be W-rich carbides with a representative EDS spectrum of an individual precipitate shown in Fig. 11D. Some V-rich carbides were also observed. The carbide distribution is relatively coarser than the samples tested at 575°C, but W and V-rich carbides are typically more coherent with the ferrite matrix than W/Fe-rich carbides. Therefore, it appears the differences in morphology are offset by the differences

in composition, coherency, and morphology resulting in similar hardness values for the samples tested at 575 and 675°C.

Mechanism of Stress-Relief Cracking

The above results show that the stress-relief cracking response of HCM2S is a balance between intergranular and intragranular carbide precipitation kinetics and load relaxation. Examination of all the samples was done postfailure. Secondary cracks and cavities were present along the prior austenite grain boundaries away from the fracture surface in each sample and the exposed grain surfaces were covered with microvoids and small particles. From the microstructural characterization, it is known that large (50 to a few hundred nm) Fe-rich M_3C carbides are mainly present at the prior austenite grain boundaries. Therefore, the particles observed on the exposed grain surfaces can be assumed to be carbides. The fracture surfaces revealed varying amounts of macroscopic ductile tearing in addition to intergranular failure. It seems logical to conclude that because both the amount of grain boundary carbides and percentage of intergranular failure increased with increasing temperature, the two are directly related. However, the failure mechanism cannot be fully explained at this point.

A simple, yet critical experiment was done to isolate the role of grain boundary carbides in these stress-relief cracking failures. Since samples tested at 575°C exhibited significant amounts of both intergranular failure and macroscopic ductile rupture, 575°C was chosen as the test temperature for this experiment. An HCM2S sample was stress-relief tested as every previous sample. However, instead of allowing the test to continue until the sample failed, the test was stopped after 2000 seconds. This time was chosen because the average time to failure for HCM2S at 575°C was 2198 seconds. The intent was to stop the test at a point after cracking had initiated and close to failure. Although many of the cracks after 2000 seconds are probably in the propagation stage, examination of this sample still provides insight into crack initiation.

Examination of the sample using light optical microscopy revealed many cracks along prior austenite grain boundaries, as shown in Fig. 12A, but no evidence of ductile rupture. This indicates failure starts by microcracks along prior austenite grain boundaries, but it does not explain how cavities initiate. Scanning electron microscopy was then used to further examine the cracks. Figure 12B and C are SEM photomicrographs of a prior austenite grain boundary showing cavities that have formed in the vicinity of M_3C carbides. Although these particles were not analyzed on this sample, knowledge of the size and distribution of precipitates along prior austenite grain boundaries from TEM analysis indicates the small particles present on the exposed grain boundaries of the fracture surfaces must be Fe-rich M_3C carbides. No other particles were found at the prior austenite grain boundaries with the exception of small W/Fe-rich carbides or a random inclusion. These findings imply cracking initiates by cavity nucleation at prior austenite grain boundary carbides. These cavities then grow, coalesce, and form microcracks. Neither cavities nor microcracks were observed at prior austenite grain boundaries devoid of carbides.

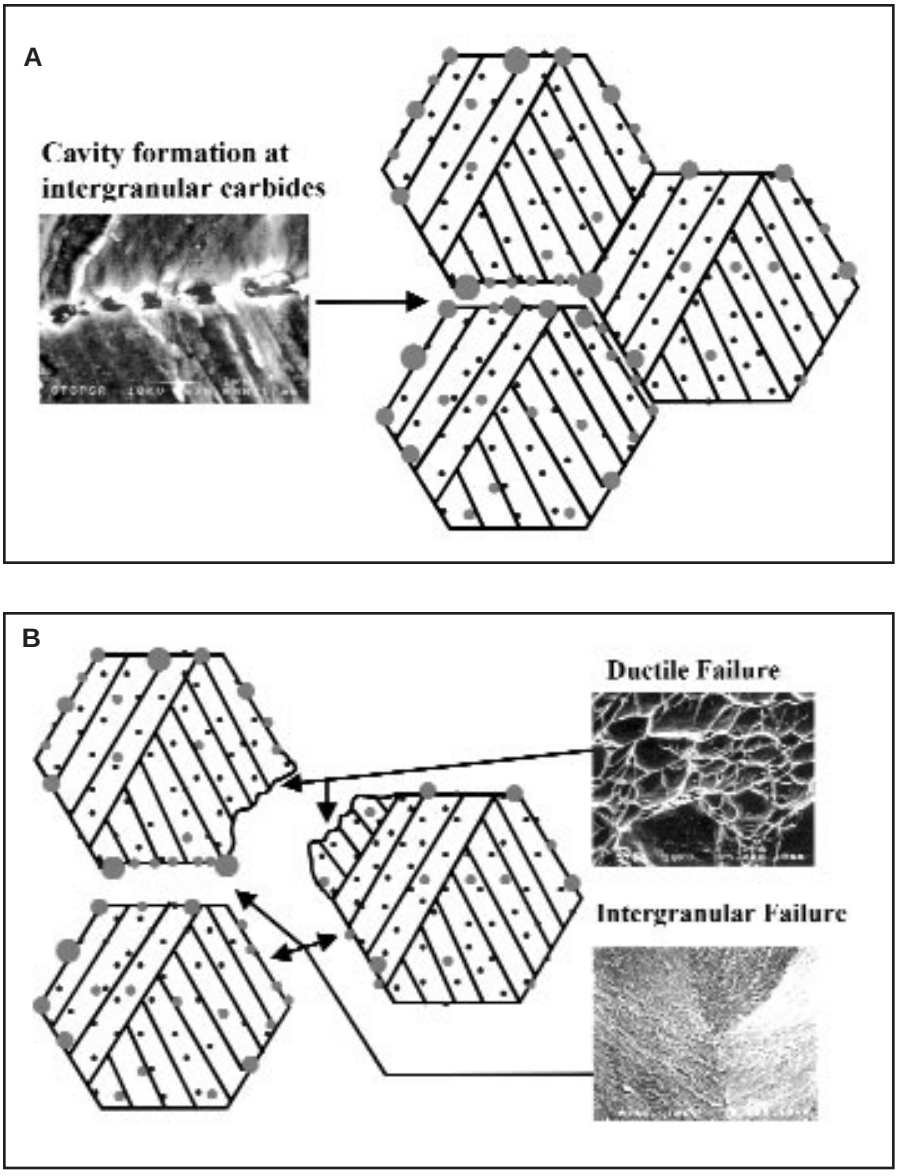

Fig. 13 — Mechanism of stress-relief cracking in the CGHAZ of HCM2S. A — During stress-relief relaxation; B — after failure.

Combining these results with the stress-relief cracking test results and microstructural characterization, the stress-relief cracking mechanism in the CGHAZ of HCM2S can be explained as schematically illustrated in Fig. 13. The mechanism is the same throughout the test temperature range, but the types of carbides and fraction of intergranular failure vary with temperature. During exposure to a PWHT temperature, Fe-rich M_3C carbides precipitate along the prior austenite grain boundaries and to a much lesser extent within the prior austenite grains. Some prior austenite grain boundaries are almost fully covered with these carbides, others are partially covered, and still others are completely devoid of these carbides. This is presumably due to the varying degree of misorientation from

boundary to boundary and along a given boundary. Some alloy carbides are also present along the prior austenite grain boundaries. These carbides also form a fine, uniform dispersion within the grain interiors both along lath boundaries and within laths. These alloy carbides provide significant precipitation strengthening. Simultaneously, the sample is held in tension at a constant displacement, which results in an applied load or stress that immediately begins to relax after the maximum load is reached. Carbide precipitation occurs simultaneously with the stress relaxation, and the rates of these two phenomena are functions of temperature.

Creep-like cavities formed during the load relaxation at M_3C/prior austenite grain boundary interfaces as illustrated in Figs. 12B and C and 13A. Eventually, these cavities linked to form microcracks along prior austenite grain boundaries. There were some grain boundaries that did not have any carbides present and therefore no cavities formed. Cavities continued to grow until enough microcracks formed and all the remaining stress was concentrated to the areas that were still intact. A point was eventually reached where the remaining uncracked areas could not sustain the stress and the material failed as conventional macroscopic ductile tearing simply due to being overstressed — Fig. 13B. This accounts for the ductile tearing shown in Fig. 3A. In addition, some grains that were only partially covered with carbides experienced both intergranular and macroscopically ductile failure at the same boundary.

The samples tested at 725°C experienced almost total intergranular failure because each prior austenite grain boundary contained many incoherent M_3C carbides. In general, these carbides were larger than those in the samples tested at 575°C. The coarser size leads to even greater incoherency because the carbides are becoming more spherical in order to minimize surface energy. Almost every prior austenite grain boundary cracked because almost every one was covered with incoherent carbides. However, the times to failure at 575, 625, and 725°C were comparable. The accelerated grain boundary weakening at 725°C relative to 575 and 625°C was offset by the increased ability of the grain interiors to plastically deform at 725°C relative to 575 and 625°C. This is the reason the times to failure were similar even though the resultant fracture surfaces were very different.

The nose of the temperature-time to failure curve occurred at 675°C. The times to failure were much shorter than any of the other test temperatures. These samples shared characteristics of both the low temperature samples (575 and 625°C) and the high temperature samples (725°C). Unfortunately, the shared characteristics were those that increase susceptibility to stress-relief cracking. Most of the prior austenite grain boundaries were covered with incoherent M_3C carbides, thus weakening the grain boundaries, as shown by the high amount of intergranular failure. The amount of intergranular failure in the samples tested at 675°C is only about 15% less than the samples tested at 725°C. A dense distribution of small intragranular W and V-rich carbides provided significant precipitation strengthening at 675°C. The intragranular hardness was approximately equal to that of the samples tested at 575 and 625°C. Therefore, the weak prior austenite grain boundary regions combined with a strong grain interior resulted in abrupt failure during the initial stages of stress-relaxation. The boundaries were covered with incoherent carbides and subsequent cavities because the grain interiors were precipitation strengthened before an appreciable fraction of the load could be relaxed. The load could then only relax through localized failure at prior austenite grain boundaries by precipitation-induced cavity initiation and propagation. This proposed mechanism explains both the C-curve behavior displayed in Fig. 1 and fracture characteristics (e.g., grain boundary cavities at precipitates and localized microvoid coalescence) of the CGHAZs of HCM2S.

Conclusions

The stress-relief cracking of a new ferritic alloy steel was investigated and a mechanism proposed based on stress-relaxation testing and detailed microstructural characterization. The coarse-grained, heat-affected zone of HCM2S was found to be susceptible to stress-relief cracking in the temperature range of 575–725°C. The stress-relief cracking susceptibility, as measured by the time to failure during stress-relaxation testing, exhibited C-curve behavior as a function of temperature when the nose of the C-curve was at 675°C. Stress-relief cracking was controlled by both intergranular and intragranular carbide precipitation. The amount of incoherent intergranular M_3C carbides increased with increasing temperature and resulted in an increase in intergranular failure. The grain interiors were resistant to plastic deformation due to precipitation strengthening by alloy carbides. Cracking initiated by cavity nucleation on incoherent, intergranular M_3C carbides. Eventually, these cavities linked to form microcracks. Complete failure occurred when the remaining uncracked areas could not sustain the load and failed due to conventional ductile tearing. Elemental segregation did not play a role in the stress-relief cracking failures. The results of this work provide a fundamental understanding of the underlying mechanisms of stress-relief cracking. In addition, this study can serve as a basis for the selection of heat treatment and welding processing variables necessary to avoid a microstructure prone to stress-relief cracking in susceptible alloys.

Acknowledgments

The authors would like to gratefully acknowledge Dave Ackland, Adam Papworth, and J. Alwyn Eades of Lehigh University for their contributions to this work.

References

1. Masuyama, F., Yokoyama, T., Sawaragi, Y., and Iseda, A. 1994. *Materials for Advanced Power Engineering*, Part I D. Coutsouradis et al., eds., Netherlands: Kluwer Academic Publishers, pp. 173–181.

2. Masuyama, F., Yokoyama, T., Sawaragi, Y., and Iseda, A. 1994. *Service Exposure and Reliability Improvement: Nuclear, Fossil, and Petrochemical Plants*. PVP, Vol. 288. ASME, pp. 141–146.

3. *Metals Handbook*,Vol. 1, 8th ed. Materials Park, Ohio: ASM International.

4. Prager, M., and Masuyama, F. 1994. *Proceedings Maintenance and Repair Welding in Power Plants V*. Orlando, Fla., pp. 16–30.

5. *Creep Rupture Data of HCM2S Steel Tubes, Pipes, Forgings, and Plates*. 1997. Sumitomo Metal Industries, Ltd., and Mitsubishi Heavy Industries, Ltd.

6. Nawrocki, J. G., DuPont, J. N., Robino, C. V., and Marder, A. R. 2000. *Welding Journal* 79(12): 355-s to 362-s.

7. Meitzner, C. F., and Pense, A. W. 1969. *Welding Journal* 48(10): 431-s to 440-s.

8. Swift, R. A., and Rogers, H. C. 1971. *Welding Journal* 50(8): 357-s to 373-s.

9. Edwards, R. H., Barbaro, F. J., and Gunn, K. W. 1982. *Metals Forum* 5(2): 119–129.

10. Irvine, K. J., Murray, J. D., and Pickering, F. B. 1960. *Journal of the Iron and Steel Institute* (10): 166–179.

11. Asbury, F. E., Mitchell, B., and Toft, L. H. 1960. *British Welding Journal* (11): 667–678.

12. Hughes, W. P., and Berry, T. F. 1967. *Welding Journal* 46(8): 361-s to 370-s.

13. Dix, A. W., and Savage, W. F. 1971. *Welding Journal* 50(6): 247-s to 252-s.

14. Dhooge, A., and Vinckier, A., 1986. *Welding in the World* 24: 104–126.

15. Meitzner, C. F. 1975. *WRC Bulletin* 211: 1–17.

16. McMahon, C. J. 1991. *Materials Characterization* 26: 269–287.

17. Dhooge, A., and Vinckier, A. 1992.

Welding in the World 30: 44–71.

18. Bika, D., Pfaendtner, J. A., Menyard, M., and McMahon, C. J. 1995. *Acta Metallurgica de Materialia* 43(5): 1895–1908.

19. Nippes, E. F., Merrill, L. L., and Savage, W. F. 1949. *Welding Journal* 28: 556-s to 564-s.

20. Nippes, E. F., and Nelson, E. C. 1958. *Welding Journal* 37: 289-s to 294-s.

21. Nawrocki, J. G. 2000. Ph.D. thesis. Lehigh University, Bethlehem, Pa.

22. *Welding Handbook*, Vol. 1, 8th ed. 1991. Miami, Fla.: American Welding Society.

23. Williams, D. B., and Carter, C. B. 1996. *Transmission Electron Microscopy*. New York, N.Y.: Plenum Press.

24. Lee, D. Y., Barrera, E. V., Stark, J. P., and Marcus, H. L. 1984. *Metallurgical and Materials Transactions* 15A: 1415–1430.

25. Titchmarsh, J. M. 1978. *Proc. 9th Inst. Congress on Electron Microscopy,* Vol I, Edited by J. M. Sturgess. Toronto, Canada: Microscopical Society of Canada, pp. 618–619.

26. Pilling, J., and Ridley, N. 1982. *Metallurgical Transactions A* 13A: 557–563.

27. Todd, J. A. 1986. *Scripta Metallurgica* 20: 269–274.

28. Read, W. T., Jr. 1953. *Dislocations in Crystals*. New York, N.Y.: McGraw-Hill Book Co., Inc.

29. Bennett, B. W., and Pickering, H. W. 1987. *Metallurgical Transactions* 18A: 1117–1122.

Preparation of Manuscripts for Submission to the *Welding Journal* Research Supplement

All authors should address themselves to the following questions when writing papers for submission to the Welding Research Supplement:

- ◆ Why was the work done?
- ◆ What was done?
- ◆ What was found?
- ◆ What is the significance of your results?
- ◆ What are your most important conclusions?

With those questions in mind, most authors can logically organize their material along the following lines, using suitable headings and subheadings to divide the paper.

1) **Abstract.** A concise summary of the major elements of the presentation, not exceeding 200 words, to help the reader decide if the information is for him or her.

2) **Introduction.** A short statement giving relevant background, purpose, and scope to help orient the reader. Do not duplicate the abstract.

3) **Experimental Procedure, Materials, Equipment.**

4) **Results, Discussion.** The facts or data obtained and their evaluation.

5) **Conclusion.** An evaluation and interpretation of your results. Most often, this is what the readers remember.

6) **Acknowledgment, References and Appendix.**

Keep in mind that proper use of terms, abbreviations, and symbols are important considerations in processing a manuscript for publication. For welding terminology, the *Welding Journal* adheres to AWS A3.0:2001, *Standard Welding Terms and Definitions.*

Papers submitted for consideration in the Welding Research Supplement are required to undergo Peer Review before acceptance for publication. Submit an original and one copy (double-spaced, with 1-in. margins on 8 ½ x 11-in. or A4 paper) of the manuscript. Submit the abstract only on a computer disk. The preferred format is from any Macintosh® word processor on a 3.5-in. double- or high-density disk. Other acceptable formats include ASCII text, Windows™, or DOS. A manuscript submission form should accompany the manuscript.

Tables and figures should be separate from the manuscript copy and only high-quality figures will be published. Figures should be original line art or glossy photos. Special instructions are required if figures are submitted by electronic means. To receive complete instructions and the manuscript submission form, please contact the Peer Review Coordinator, Doreen Kubish, at (305) 443-9353, ext. 275; FAX 305-443-7404; or write to the American Welding Society, 550 NW LeJeune Rd., Miami, FL 33126.

Do You Have Some News to Tell Us?

If you have a news item that might interest the readers of the *Welding Journal*, send it to the following address:
Welding Journal Dept.
Attn: Mary Ruth Johnsen
550 NW LeJeune Rd.
Miami, FL 33126.
Items can also be sent via FAX to (305) 443-7404 or by e-mail to *mjohnsen@aws.org*.